Available online at www.sciencedirect.com

ScienceDirect

Procedia CIRP 126 (2024) 987–992

www.elsevier.com/locate/procedia

17th CIRP Conference on Intelligent Computation in Manufacturing Engineering (CIRP ICME '23)

Structured-light 3D Scanning Performance in Offline and In-process Measurement of 3D Printed Parts

Moustapha Jadayel*, Farbod Khameneifar

Polytechnique Montréal, 2500 Chem. De Polytechnique, Montréal, QC H3T 1J4, Canada

* Corresponding author. *E-mail address:* moustapha.jadayel@polymtl.ca

Abstract

This paper presents a geometric analysis comparison of structured-light 3D scanners against coordinate measuring machines (CMMs) in measuring 3D printed plastic parts. The resulting geometric analysis of a 3D printed part measured with a contact probe on a CMM and measured with a structured light 3D scanner is presented, along with an error analysis that includes a statistical comparison of the measured geometric deviation. This analysis is then used to determine if structured-light 3D scanners are reliable enough to perform a GD&T analysis of specific features. This paper also presents the results of in-process 3D scanning and compares them to offline 3D scanning to determine the suitability of in-process 3D scanning for comprehensive analysis of geometric deviation and GD&T features.

Keywords: Structured-light 3D scanner; Coordinate measuring machine (CMM); 3D Printing; In-process 3D scanning; Geometric inspection; Quality control

1. Introduction

Additive manufacturing (AM), or 3D printing, has revolutionized the production of complex and intricate parts across various industries [1]. While AM offers numerous benefits, including faster prototyping, reduced material waste, and increased design freedom, it also poses unique challenges regarding quality control [2]. Traditional methods for measuring the accuracy of manufactured parts, such as coordinate measuring machines (CMMs), are time-consuming and costly, reducing the efficiency of rapid prototyping or low-volume production. As a result, CMMs may not be adequate to analyze the geometry of a 3D printed part promptly, especially for parts with intricate features and shapes.

Structured-light 3D scanning is a promising alternative for measuring 3D printed parts, offering faster results than traditional methods [3]. In structured-light 3D scanning, a pattern of light is projected on the surface of an object, and two cameras capture the distortion at a calibrated distance and angle between them. The difference in the captured pattern is used to reconstruct the object's geometry [4]. The result of 3D scanning is a disorganized point cloud of the surface of the measured part, which can then be used for geometric inspection.

Without a recognized standard procedure to compare the different technologies, several researchers have developed methods and artifacts to evaluate the metrological performance of structured light 3D scanning [5, 6, 7]. Additionally, 3D scanner manufacturers also create their own evaluation artifacts that the end-user can use to verify the quality of their equipment.

This scan-based inspection result can also be used to compensate the geometry of parts to improve their geometric accuracy [8]. It is also possible to optimize the quality control process for speed even more by integrating measuring sensors in the 3D printing process [9, 10].

10.1016/j.procir.2024.08.372

In this paper, we present a measurement comparison of a 3D printed Polylactic Acid (PLA) part using a CMM and a structured-Light 3D scanner. We also present an in-process 3D scanning measurement and evaluate the variation of the measurements at different layers of the printing process. This study investigates the metrological performance of structured-light 3D scanning for the geometric inspection of 3D printed parts. By comparing the results of in-process and offline 3D scanning and CMM measurement, we aim to provide insights into the accuracy and reliability of offline and in-process structured-light 3D scanning as a quality control tool for AM.

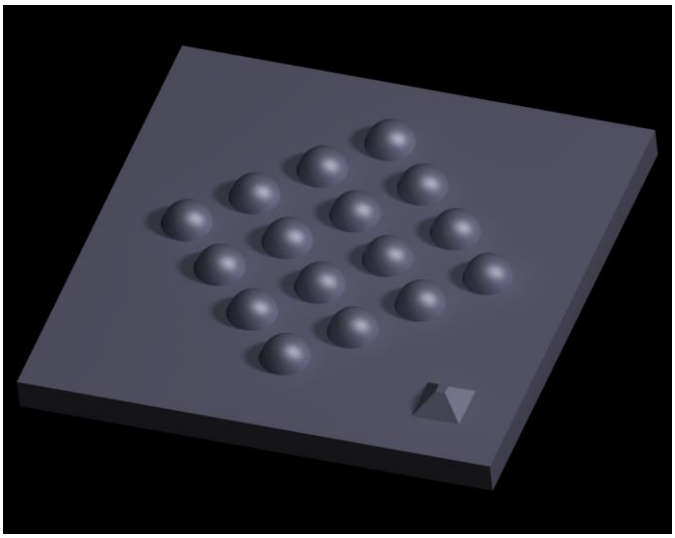

Figure 1: 3D model of the ball plate used for the analysis.

2. Methodology

2.1. Part Fabrication

The part used in this study is a plate with 16 spheres arranged in a diamond pattern. A feature to help determine the part's orientation is present on the corner used as the origin of the measurement coordinate system. A representation of the part used is presented in Figure 1. Spheres were chosen as the measured features due to their simple geometry, which is amenable to numerical analysis. The overall size of the part is 75 mm x 75 mm in length and width. The plate is 5 mm thick, and the radius of the spheres is 3.75 mm. The size is representative of the usual parts printed by a desktop 3D printer.

The part is printed, with white PLA, on a *Prusa i3 MK3S* (Prusa, Prague, Czech Republic.) modified to allow for in-process 3D scanning. The geometry was sliced using the Cura slicing software with default fast parameters. The main parameters of these settings are presented in Table 1. The accuracy reported by the printer's manufacturer is 0.1 mm on the Z-axis and 0.3 mm on X and Y axes [11].
The same part is measured by CMM, offline 3D scanning, and in-process 3D scanning, where the part is scanned at every five layers during the printing process. More details on the in-process 3D scanning will be presented in section 2.4.

Table 1: Printing parameters of the measured part.

Printing parameters	Value
Printing temperature	200 °C
Build plate temperature	60 °C
Layer height	0.2 mm
Infill density	20 %
Printing speed	60 mm/s

2.2. CMM Measurement

The part is measured with a Coordinate Measuring Machine (CMM) following the printing and in-process scanning. The machine used for this study is a Mitutoyo Legex 960 (Mitutoyo, Kawasaki, Japan) equipped with a TP7M probe (Renishaw, Wotton-under-Edge, United Kingdom). The length of the stylus is 20 mm, and the radius of the tip is 2 mm. This measurement dataset offers a theoretically reliable and precise measurement of the printed part. For this reason, it is used as a reference for the other measurements. Each sphere is measured using 51 measurement points covering the whole surface of each sphere for a total of 816 measurement points.

Next, the measurement dataset is processed using a Python script. This script separates the dataset into 16 groups according to what feature it measures and fits a sphere to each. To eliminate any registration errors due to the origin being measured by the CMM on the part, an additional registration transformation is applied by using Procrustes' analysis [12] with the center of the fitted spheres and the nominal sphere centers from the CAD model.

2.3. Offline 3D Scanning

The printed part is then scanned using an optical structured light 3D scanner. This study uses the Atos Core 200 (GOM, Braunschweig, Germany) with *GOM Scan*, its data acquisition software. The part is installed rigidly on a manual turntable with scan markers, easily detectable by the 3D scanner. The part is rotated and scanned to capture the geometry from all sides. Thanks to the markers installed on the turntable, the software can accurately stitch multiple scans to form the complete point cloud of the entire part. Figure 2 shows the part on the turntable scanned with the Atos Core 200 3D scanner.

The resulting point cloud consists of approximately 525,000 points with a resolution of around 72.5 points/mm^2. The data was then exported to *GOM Inspect* for registration with the nominal geometry. A Python script then isolates the points related to the spheres from the rest of the point cloud and fits spheres to them.

2.4. In-Process 3D Scanning

The process of scanning the part while it is being printed required modifications to the 3D printer. The *Prusa i3 MK3S*

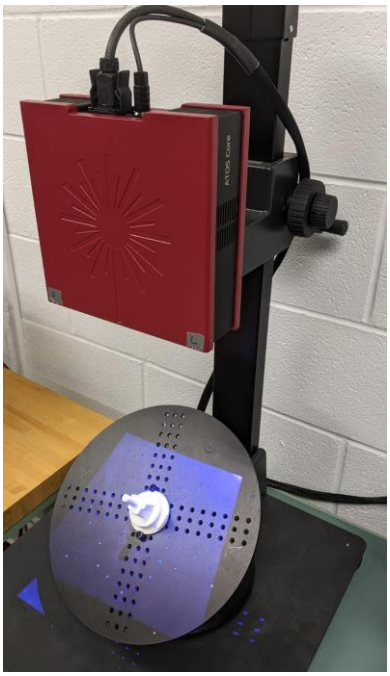

Figure 2: Offline 3D scanning setup

was modified to include a flat bearing and a pulley under the build plate to allow precise and smooth rotation. A NEMA 17 stepper motor and an *Arduino Uno* (Arduino, Turin, Italy) microcontroller were also added to control the rotation according to serial commands sent from the controlling computer. The 3D scanner used for in-process 3D scanning is the *Atos Core 200,* which is used for offline 3D scanning.

Every five layers, the printer receives a stop command and moves the print head to a position on the edge of the scanning volume, and the build plate moves to the center of the scanning volume. Then, the build plate and everything on it are scanned multiple times in different orientations to complete 360 degrees of coverage. Scan markers are placed on the print bed for the 3D scanner software to compute the exact orientation and position of the bed. Figure 3 shows the modified 3D printer in its scanning position.

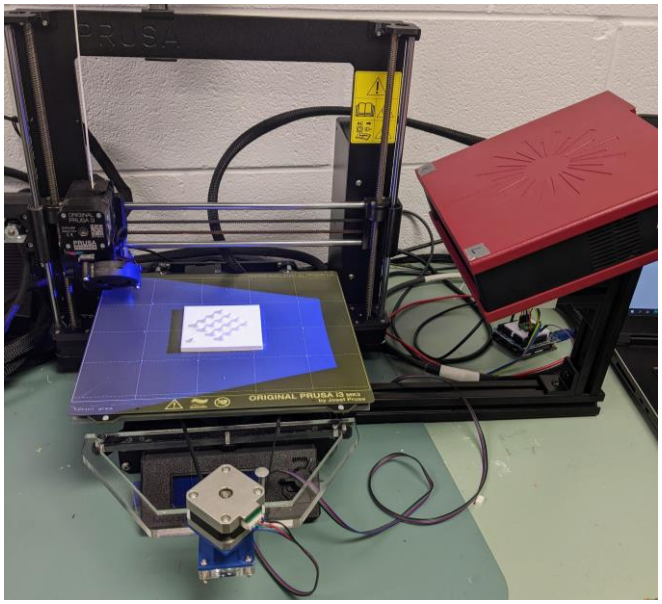

Figure 3: In-process 3D scanning setup in the scanning position.

The output of the in-process 3D scan is eight point clouds made of 312,000 points for the first scanned layer to 416,000 points for the last scanned layer. Each scanned layer captures the outside geometry and the visible infill at that layer. A Python script filters the extraneous points in the point cloud, isolates the points corresponding to each sphere and computes a fitted sphere to each.

3. Offline 3D Scan vs CMM Analysis

When analyzing the offline 3D scan dataset, the CMM measurement is taken as the reference geometry, as it offers an accurate representation of the printed part, which we use to characterize the measurement errors produced by the 3D scanner. This analysis focuses on the error in distance measurement, the error in size measurement and the error in form measurement.

3.1. Error in Distance Measurement

The distance between the center of each two fitted spheres is measured, and the error in distance measurement is the difference between the distance measured with the 3D scanner data and the distance measured with the CMM data. There are $n(n-1)/2$ unique combinations in a set of n elements; with 16 spheres, we obtain 120 distance values. Equation 1 demonstrates the error in distance measurement e_{dist}^{uv} as defined in this study.

$$e_{dist}^{uv} = \|c_{Scan}^{u} - c_{Scan}^{v}\| - \|c_{CMM}^{u} - c_{CMM}^{v}\| \qquad (1)$$

Where c_{Scan}^{u} and c_{Scan}^{v} are the center of fitted sphere u and v from the scan data and c_{CMM}^{u} and c_{CMM}^{v} is the center of fitted sphere u and v from the CMM data. Figure 4 shows the measurement errors for each nominal distance. The average error is 0.017 mm with a standard deviation of 0.029 mm. The Root Mean Square (RMS) value is also calculated to be 0.033 mm.

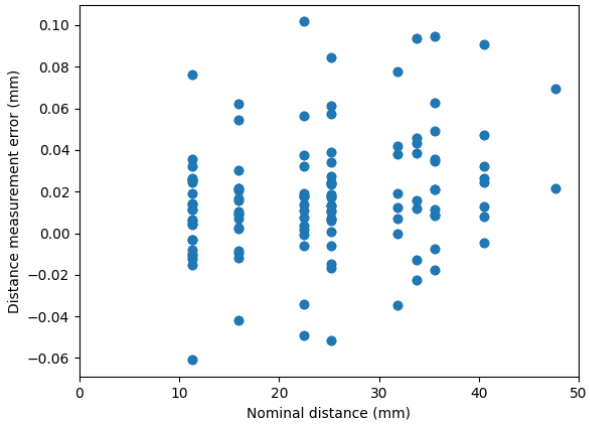

Figure 4: Error in distance measurement.

3.2. Error in Size Measurement

The size measurement is the radius of the fitted sphere and the error in size measurement is the difference between the size measured with the 3D scanner and the size measured with the CMM. The error in size measurement e^i_{size} is computed using equation 2.

$$e^i_{size} = r^i_{scan} - r^i_{CMM} \quad (2)$$

Where r^i_{scan} is the radius of fitted sphere i in the scan dataset and r^i_{CMM} is the radius of fitted sphere i in the CMM dataset. The average error in size measurement is -0.095 mm with a standard deviation of 0.030 mm. The maximum error calculated is -0.159 mm, and the minimum error is -0.053 mm.

3.3. Error in Form Measurement

The form measurement is represented by the fitted residuals of the fitted spheres. The error in form measurement is taken as the difference of the average of fitted residuals between each corresponding spheres from the scan and the CMM dataset. Equation 3 demonstrates the fitted residual $form^i_{scan}$ of sphere i in the scan dataset. The fitted residual $form^i_{CMM}$ is calculated with the same equation using the CMM dataset instead. Equation 4 shows the error in form measurement e^i_{form} of sphere i.

The distinction between the size measurement and the form measurement is that the latter offers information on how well the measured points form a sphere while the former informs us on what sphere represents the given points optimally.

$$form^i_{scan} = \frac{\sum_j^{n_{scan}} \left\| p^{j,i}_{Scan} - c^i_{Scan} \right\|}{n^i_{Scan}} - r_i \quad (3)$$

$$e^i_{form} = form^i_{scan} - form^i_{CMM} \quad (4)$$

Where $p^{j,i}_{Scan}$ is the position of point j of sphere i in the scan dataset, c^i_{Scan} is the position of the center of fitted sphere i, n^i_{scan} is the number of points corresponding to sphere i in the scan dataset and r_i is the radius of fitted sphere i.

The error in form measurement for the printed part is, on average 0.010 mm and its standard deviation is 0.008 mm. The RMS for this error is 0.099 mm. After analyzing the data, it appears that the unusually high value for the RMS is the result of an outlier error on sphere 14. The form measurement error for this outlier is 0.039 mm. However, by excluding the error from this fitted sphere, we were able to obtain a new average of 0.008 mm, a standard deviation of 0.003 mm, and an RMS value of 0.008 mm. Upon further inspection, it seems that sphere 14 has a blob of solidified material that went undetected by the CMM.

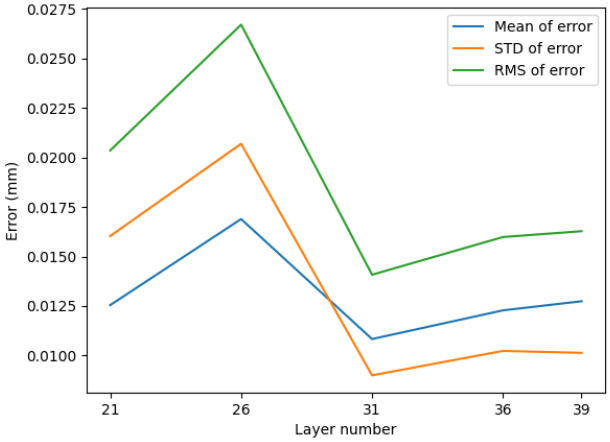

Figure 5: Mean, standard deviation (STD) and Root mean square (RMS) of the distance measurement error on scanned layers.

4. In-Process 3D Scan vs Offline 3D Scan Analysis

In this section, the in-process 3D scan dataset is compared to the offline 3D scan of the same part. The offline scan is chosen as the reference data to determine if in-process 3D scanning is reliable to inform decisions on the accuracy of the 3D printed part before it is finished. As the in-process scan occurs at multiple layers, the analysis is conducted on multiple point clouds obtained at different layers, and their trends are compared to the offline scan.

4.1. Error in Distance Measurement

The error in distance measurement is computed similarly to equation 1, with the difference that the offline 3D scanner dataset is now the reference, taking the place of the CMM dataset. Also, the in-process 3D scanner dataset is the dataset to analyze, instead of the scan dataset from Equation 1.

Theoretically, the position of the spheres, and the distance between them, should not change between each measurement. In reality, the computed position of the fitted spheres changes

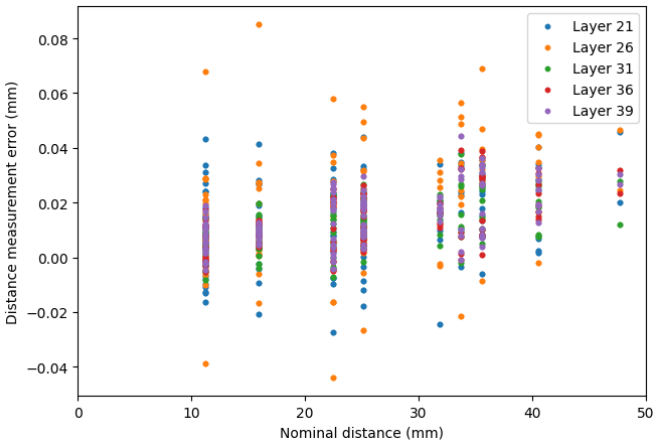

Figure 6: Error in distance measurement at each scanned layer.

from one scanned layer to another because of imperfections on the surface of the spheres which affect the computation of the fitted spheres. Additionally, imperfection on early layers of the part has a proportionally more important effect on the fitted spheres. Figures 5 and 6 show the trend of the error of the distance between spheres and it suggests that before layer 31 the data is not reliable enough to determine the geometric quality of the printed part.

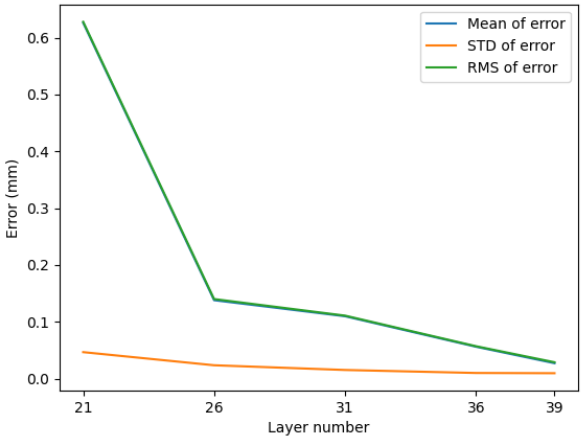

Figure 7: Mean, Standard deviation (STD) and Root mean square (RMS) of the size measurement error on scanned layers. Note that the mean and RMS curves appear superimposed due to the scale of the chart being much larger than the difference between the two curves.

4.2. Error in Size Measurement

The size measurement error is analyzed to determine the accuracy of the 3D scanner when measuring size features on a printed part. Equation 2 is adapted by using the offline 3D scan as the reference data instead of the CMM data and the in-process 3D scan as the data to evaluate instead of the offline 3D scan data. The adapted equation is then used to compute the error in size measurement between the in-process 3D scanning and the offline 3D scanning.

For the in-process 3D scanning, the variation of the computed error in size measurement demonstrates that scans from early layers are most impacted by missing data and geometric deviation from the printer, as they disproportionately affect the results.

Figure 7 displays the progress of the error in size measurement. It is clear from this figure that the error is indeed greater in the first scanned layers than in the last two layers. In addition, we can notice that the standard deviation of the error is much smaller than the mean and RMS, which shows that there may be a systematic error common in all spheres.

4.3. Error in Form Measurement

The error in form measurement is important to analyze as it can help to determine if the form measurement is reliable. Equations 3 and 4 are adapted in the same manner than the other two equations, by replacing the offline 3D scan as the reference data instead of the CMM data and the in-process 3D scan as the data to evaluate instead of the offline 3D scan data. Adapted equations 3 and 4 are then used for the error computation with the offline 3D scan as the reference measurement and the in-process 3D scan as the measurement to analyze. This analysis will also be highly influenced by

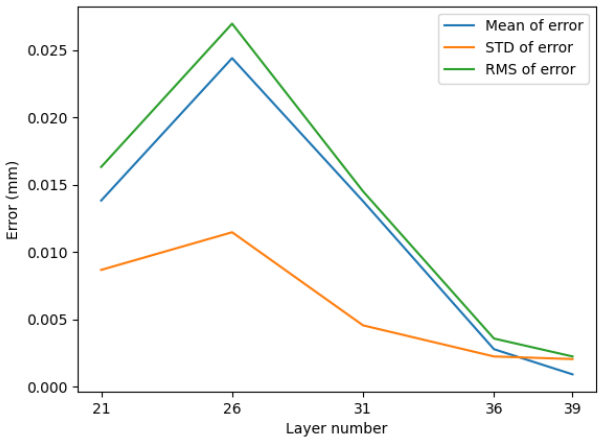

Figure 8: Mean, standard deviation (STD) and Root mean square (RMS) of the form measurement error on scanned layers.

missing data and printing errors causing it to be unreliable in early layers.

Figure 8 shows the evolution of the form error across the scanned layer. From the figure, we can observe that the layers before layer 36 have a much higher error in form measurement than the last couple of layers. That is what we expect from having more data points on which we fit spheres.

5. Discussion

It is clear from the results of the offline scan to CMM analysis, shown as a summary in table 2, that the 3D scanner can accurately capture the geometric quality of a 3D printed part. However, further assessment is required to define the measurement uncertainty of the 3D scanner data. Notably, the mean error in size measurement is higher than the other measurement errors. This higher value is likely due to a previously undetected systematic error in the measurement of the 3D scanner.

Table 2: Summary of the measurement error of the offline 3D scanner to CMM analysis.

Measurement type	Mean error (mm)	Standard deviation of error (mm)	Root Mean Square of error (mm)
Distance	0.017	0.029	0.033
Size	-0.095	0.030	0.100
Form	0.010	0.008	0.099

On the other hand, CMMs can only measure at predetermined points on the surface of the part and can easily miss errors on the part due to the low number of measurement points. This is what we see in section 3.3, where a blob of extra material was present on the surface of the sphere. This blob was accurately captured by the 3D scanner, but not the CMM. On the other hand, if the CMM had detected it, it would have had a more significant impact on the quality of the measurement due to the relatively high impact of each measurement point.

On the comparison of the in-process 3D scanning and the offline 3D scanning, we see that all errors are high in early layers, meaning the scan data is not reliable to use as an early prediction of final geometric deviation. Nevertheless, using statistical analyses, could determine if a certain tolerance on a scanned feature would not be respected early in the printing process, reducing wasted material and time. However, a custom statistical model may be required for each feature type. A machine learning model could also be used to compute the probability of a tolerance being respected.

Additionally, we can compare the measurement errors of the last layer of the in-process 3D scan to the offline 3D scan measurement errors, as the scanned part is finished in both measurements. This comparison shows that the distance, size, and form errors are small relative to earlier layers, most likely due to thermal deformation. It could also be attributed to the error of repeatability of the 3D scanner. Furthermore, the offline 3D scanned part was carefully scanned to capture all sides of all spheres and leave as few holes as possible. That is something that would not be possible to guarantee for the in-process 3D scan. This fact could have decreased the quality of the in-process measurement.

Conclusion

This study shows that the 3D scanner can accurately capture the geometric accuracy of the 3D printed part and that the 3D scanner has the significant advantage of being able to capture the entirety of the surface of the geometry without requiring a significant amount of time. However, additional investigation is needed to determine the measurement uncertainty of 3D scan data.

For in-process 3D scanning, the automation of the scanning process before being removed from the 3D printer brings the same advantages as offline 3D scanning in addition to the possibility of adjusting the printing process by compensation. Despite that, more extensive research is needed to refine the acquired data to obtain similar results to offline 3D scanning.

Finally, further research should be conducted to improve the efficiency of in-process 3D scanning. Also, more quality control methods could be integrated with the proposed setup to develop a complete analysis of the geometric accuracy of the printed part and other properties that could be verified, i.e., porosity, surface roughness, or the quality of the infill.

Acknowledgments

The authors wish to express their gratitude for the financial assistance provided by the Natural Sciences and Engineering Research Council of Canada (NSERC) and the Fonds de Recherche du Québec Nature et Technologies (FRQNT).

References

[1] Khorasani, M., Ghasemi, A., Rolfe, B., & Gibson, I. (2021). Additive manufacturing a powerful tool for the aerospace industry. Rapid Prototyping Journal, 28(1), 87–100. https://doi.org/10.1108/RPJ-01-2021-0009

[2] Kim, H., Lin, Y., & Tseng, T.-L. B. (2018). A review on quality control in additive manufacturing. Rapid Prototyping Journal, 24(3), 645–669. https://doi.org/10.1108/RPJ-03-2017-0048

[3] Wang, R., Law, A. C., Garcia, D., Yang, S., & Kong, Z. (2021). Development of structured light 3D-scanner with high spatial resolution and its applications for additive manufacturing quality assurance. The International Journal of Advanced Manufacturing Technology, 117(3), 845–862. https://doi.org/10.1007/s00170-021-07780-2

[4] Rocchini, C., Cignoni, P., Montani, C., Pingi, P., & Scopigno, R. (2001). A low cost 3D scanner based on structured light. Computer Graphics Forum, 20(3), 299–308. https://doi.org/10.1111/1467-8659.00522

[5] Ghandali, P., Khameneifar, F. and Mayer, J.R.R., (2019). A pseudo-3D ball lattice artifact and method for evaluating the metrological performance of structured-light 3D scanners. Optics and Lasers in Engineering, 121, pp.87-95.

[6] Bonin, R., Khameneifar, F., & Mayer, J. R. R. (2021). Evaluation of the metrological performance of a handheld 3D laser scanner using a pseudo-3D ball-lattice artifact. Sensors, 21(6), 2137.

[7] Cuesta, E., Meana, V., Álvarez, B. J., Giganto, S., & Martínez-Pellitero, S. (2022). Metrology Benchmarking of 3D Scanning Sensors Using a Ceramic GD&T-Based Artefact. Sensors, 22(22), 8596. https://doi.org/10.3390/s22228596

[8] Jadayel, M., & Khameneifar, F. (2020). Improving geometric accuracy of 3D printed parts using 3D metrology feedback and mesh morphing. Journal of Manufacturing and Materials Processing, 4(4), 112.

[9] Sun, W., Zhang, Z., Ren, W., Mazumder, J., & Jin, J. (Judy). (2022). In Situ Monitoring of Optical Emission Spectra for Microscopic Pores in Metal Additive Manufacturing. Journal of Manufacturing Science and Engineering, 144(1), 011006. https://doi.org/10.1115/1.4051532

[10] Qin, J., Hu, F., Liu, Y., Witherell, P., Wang, C. C. L., Rosen, D. W., Simpson, T. W., Lu, Y., & Tang, Q. (2022). Research and application of machine learning for additive manufacturing. Additive Manufacturing, 52, 102691. https://doi.org/10.1016/j.addma.2022.102691

[11] FAQ - Frequently Asked Questions | Prusa Knowledge Base. (n.d.). Retrieved April 6, 2023, from https://help.prusa3d.com/article/faq-frequently-asked-questions_1932

[12] Gower, J. C. (1975). Generalized procrustes analysis. Psychometrika, 40(1), 33–51. https://doi.org/10.1007/BF02291478